↑ 2㎝ ↓	An Edible Quasi-Solid Electrolyte Derived from Agarose Gel for High-Performance,Flexible Supercapacitors	
↑ 2.5㎝ ↓	2015년	
↑ 4㎝ ↓		
↑ 3㎝ ↓	문원균	
↑ 2㎝ ↓		

공학석사 학위논문

An Edible Quasi-Solid Electrolyte Derived from Agarose Gel for High-Performance, Flexible Supercapacitors

한천을 이용한 식용 준고상 젤 전해질 합성 및 휘어지는 고성능 수퍼커패시터로의 적용

2015년 2월

서울대학교 대학원

화학생물공학부

에너지환경화학융합기술전공

문원균

공학석사 학위논문

An Edible Quasi-Solid Electrolyte Derived from Agarose Gel for High-Performance, Flexible Supercapacitors

한천을 이용한 식용 준고상 젤 전해질 합성 및 휘어지는 고성능 수퍼커패시터로의 적용

2015년 2월

서울대학교 대학원

화학생물공학부

에너지환경화학융합기술전공

문원균

An Edible Quasi-Solid Electrolyte Derived from Agarose Gel for High-Performance, Flexible Supercapacitors

지도교수 이 종 협

이 논문을 공학석사 학위논문으로 제출함
2015 년 2 월

서울대학교 대학원
화학생물공학부
문 원 균

문원균의 공학석사 학위논문을 인준함
2015 년 2 월

위 원 장 성 영은 (인)

부위원장 이 종협 (인)

위 원 김 대 형 (인)

Abstract

An Edible Quasi-Solid Electrolyte Derived from Agarose Gel for High-Performance, Flexible Supercapacitors

Won Gyun Moon

School of Chemical and Biological Engineering

The Graduate School

Seoul National University

As one of the energy storage devices (ESD), supercapacitors have attracted considerable attention with their remarkable advantages such as fast charge-discharge rate, long cycle life, and environmental friendliness in nature. To improve their performance in terms of higher energy and power densities, their unit components, such as an electrolyte and electrode materials, have to be improved in preference. In particular, electrolyte serves as an ion transport media between anode and cathode as well as being a key parameter for deformable attributes in cell configuration. Therefore, a focused study on the electrolyte geometry allows further pursuit of application, in accordance with current demand for transformable compact power sources. Consequently, development of suitable electrolyte should be oriented under the notion of combining high performance and shape adapting features, mild synthesis condition involving negligible vapor pressure and flame retardancy.

Agarose gel is a soft, deformable waterborne gel, featuring high elasticity and eco-friendliness with low costs. Inside such agarose based hydrogels, the interconnected porous network filled with an aqueous medium provides an ion

reservoir, hence facilitating the diffusion of charged molecules (DNA, proteins and ions) under an electric field. On the basis of this phenomenon, agarose-based hydrogels have been widely used in the fields of food production, biological research and various gel-based electronic devices. However, practical applications of agarose gels as an electrolyte material in supercapacitor configurations have not been reported. The dissertation referred to herein, contains physico-chemical characterization of supercapacitor assembled with agarose-NaCl hydrogel and MnO_2 electrodes, with focusing on a finding optimal status of electrode, optimal synthetic conditions of electrolyte based on facile fabrication steps to exhibit desirable performance in flexible supercapacitor.

The findings show that employing agarose-NaCl gel electrolyte within the assembly of supercapacitor has noticeable advantages: (1) the preparation of the gel electrolyte consists of relatively simple steps such as solution-mixing, heating and casting in moderate conditions, which are facile, non-toxic and cost competitive fabrication. (2) The shape of the gel, including size and thickness, can easily be tuned by using razor blade method and the number of glass blocks. Furthermore, with the aid of foresaid gadgets, the gel can be transferred onto most of substrates regardless of material types such as glass, stainless steel and plastic plates, which reveals the use of such gel is industrially feasible. (3) Flexible supercapacitor can be fabricated by introducing the polymeric current collector and our gel together. This assures the gelation-based full cell build-up of a promising method for the fabrication of enlarged flexible devices.

On the basis of above-mentioned process, the supercapacitor incorporating NaCl - agarose gel electrolyte was assembled. The as-prepared agarose hydrogel consists of a 3-dimensionally interconnected agarose backbone and inter-particular submicropores filled with water and sodium, chloride ions. As a framework, the agarose matrix provides structural stability of the gel electrolyte. Furthermore, the developed porous networks with the water filler provide an efficient ion transport pathway between anode and cathode electrodes. In accordance with these properties, the quasi-solid gel facilitates the assembled supercapacitor to have a specific capacitance of 286.9 F g^{-1} under a MnO_2 symmetric cell, and high rate capability that is 80 % of specific capacitance compared to a liquid electrolyte (NaCl aqueous solution) at a scan

rate of 100 mV s^{-1}. In addition, linking with high capacitive performance, the gel electrolyte features highly scalable, cost effective, safe and environment-friendly characteristics, which are attributed to the simple procedure and easily available components of the agarose gel. Hence, we concluded that the developed quasi-solid gel is promising material for use in various energy storage and delivery systems.

Keywords: electrochemistry, supercapacitor, quasi-solid gel electrolyte, agarose hydrogel

Student Number: 2013-22522

Contents

List of Figures

List of Figures

Chapter 1. Introduction

1.1 Supercapcitor

As one of the consequences of the global warming and energy crisis, the appetite for enhanced energy storage devices (ESD) with higher energy and power densities has been increased considerably. Among the various forms of ESD, supercapacitors are highlighted by virtue of their outstanding features that include a fast charge-discharge rate, long cycle life, and environmental friendly nature [1-3].

Supercapacitors are classified into two main categories, electrochemical double layer capacitors (EDLCs) and pseudocapacitors. Firstly, EDLCs store charge on the interface between electrode and electrolyte as an electrical double layer [4, 5]. Solvated electrolyte ions are attracted to the electrode surface by equal magnitude of opposite charges on the electrode resulting two capacitors series connected by electrolyte. With combination of high electrode surface area and the nanoscale thickness of the double layer, EDLCs exhibit several orders of magnitude higher than those of electrostatic capacitors in terms of capacitance and energy density. Secondly, pseudocapacitors, compared to EDLCs, performs fast, potential-dependent reactions stem from Faradaic charge transfer across the double-layer [6-11]. These pseudocapacitive reactions are thermodynamically favored in certain ranges of potential, exhibiting capacitive characteristics on that boundaries. The illustrative mechanism of EDLC and psuedocapacitor are shown in Fig. 1-1 [2, 12]. In

general, capacitive behavior is identified with cyclic voltammetry. Materials performing only double-layer capacitance manifest parallelogram-shaped voltammogram profiles, on the other hand pseudocapacitive materials generate irregular peaks.

On the regard of comparing ESD performances, the reversibility of the chemical and capacitive ESD is dramatically different. Charge transfer across the electrode and electrolyte interface gives rise to changes in the structure of the electrode by redox reactions and reduces cycle life in batteries. Whereas, the charge storage mechanism in EDLCs has no related chemical changes during cycle, resulting a highly reversible charge storage and cycling [13, 14]. This difference is usually summarized in a Ragone plot with energy density ((W h) kg^{-1}) and power density (W kg^{-1}). Fig. 1-2. displays a Ragone plot comparing the energy and power densities of Li-ion batteries and ECs. ECs are able to produce much higher power densities compared to batteries, and exhibit considerably reduced material stability problems with safety [15-20].

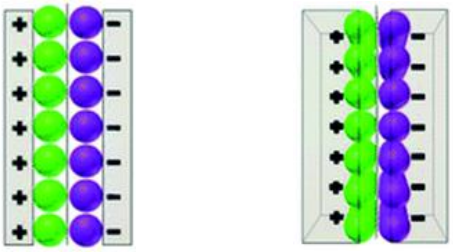

Figure 1-1. Illustrative representations of EDLC where charges are separated at the electrode/electrolyte interface (Left), a pseudocapacitor where charge transfer reactions occur on the electrode surface (Right) [2].

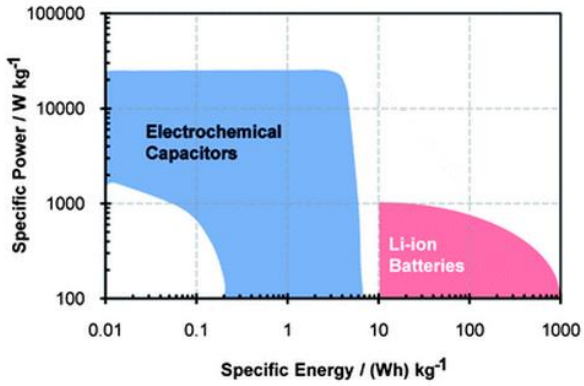

Figure 1-2. Ragone plot of ECs and high-power Li-ion batteries [2].

1.2 Ion gel system

Commonly, liquid electrolytes such as acid, alkali solution are applied to conventional supercapacitors, which show similarities to batteries [21, 22]. On the other hand, critical issues hinder further applications of this configuration. The use of liquid makes supercapacitor heavy causing difficulties of its integration, and to avoid electrolyte leakage requires safe encapsulation, leading to increase of costs [21, 23]. Therefore, solid polymer electrolytes (SPEs) have been developed for substituting liquid electrolyte.

In respect of the expanding demand for portable, flexible ESD, SPEs based supercapacitors are regarded as potential prime candidates. To compensate the drawbacks of liquid electrolytes, SPEs-based full-cell configuration assures a supercapacitor would store and provide electrical energy with having enough capacity to endure certain levels of deformation [22]. Typical SPEs are produced with direct dissolving salts such as, $LIPF_6$, $LiBF_4$ and $LiClO_4$, into an ion-coordinating polymer such as PEO (polyethylene-oxide), siloxane, and copolymers derived from them [24, 25]. Such typical systems have been widely studied, and preparation techniques like solvent casting, extrusion, lamination, or even by in situ polymerization also have been developed [25]. Though, owing to their poor conduction nature, the low electrochemical performance of SPEs configuration impedes their expansion of various applications. This crucial limitation, came from the relatively low ionic conductivity at room temperature ($10^{-8} < \sigma < 10^{-3}$ S cm^{-1}) [26, 27], causes increased internal resistance and reduced charge storage features, compared to liquid electrolyte

configuration [21]. An adequate design of the electrode-electrolyte interface along with ionic conductivity is one of the primary factor in energy storage and conversion systems in ESDs, and it will contribute in achieving excellent electrochemical performance in the future. Thus, a well designed electrolyte geometry that can ensure optimal electrode-electrolyte interface contact with efficient ionic transport is under both scientific and practical significance.

Ion gels are polymeric networks swollen with an ionic liquid [28, 29], representing main candidates with fusing the key merits of liquid and solid polymer electrolytes. The cohesive solid character with liquid-like transport properties, would expected to offer a suitable configuration because of their virtue of a high degree of flexibility including semi-solid characteristics as well as high ionic conductivity [21, 22, 25]. Conventional ion gel systems such as PVA-H_3PO_4, PVA-H_2SO_4, PAN-PEG-$LiClO_4$, P(VDF-HFP)-$EMIMBF_4$ have been reported [26, 30-33]. Theses polymer-ionic liquid combinations exhibit mechanical deformability and high performance with a low probability of safety problems, owing to process applied in their fabrication [29, 30, 34, 35]. The high cost of synthesis and environmental impact with toxicity concerns, however, related to ion-gel chemicals are drawbacks for their plausible use.

1.3 Agarose gel

An agarose-based hydrogel consists of agar with an agarobiose monomeric unit, featuring sub-micrometer pores (pore sizes of 400-500nm), a high elasticity (Young's modulus of 116 kPa) with low cost and environmentally benignity [36-40]. The agarose gelation contains the crosslinking self-assembly of molecules via hydrogen bonding [41], and resulting the formation of a semi-solid waterborne gel with a 3D porous structure [42]. Owing to the high water content of 90% in weight proportion and interconnected hierarchical pore structure, the agarose hydrogel is a soft, moldable and bio-compatible medium with high ion mobility [43]. Moreover, as one kind of ion gel, the ionic attributes of the agarose gels can be modified by the introduction of an ionic liquid as a functional filler with negligible vapor pressure, non-volatility and flame retardancy.

On the basis of above-mentioned features, agarose-based hydrogels have been widely applied in the fields of food production, biological research [44, 45] to various gel-based device systems such as ion current diode [46], a memristor [47], a photovoltaic device [43], and a polyelectrolyte diode [48, 49]. To the best of our knowledge, on the other hand, researching practical applications of agarose gels as an electrolyte material in supercapacitor configurations have not been reported yet. In addition, retaining their electrochemical performance with enhanced mechanical flexibility and environmental benignity of electrolytes continues to be a challenge.

1.4 Objectives

This thesis report on a high performance quasi-solid gel (NaCl-Agarose gel) for use in flexible supercapacitors under the incorporation of a sodium chloride ion pair into a hydrogen bonded cross-linking agarose gel. The 3D porous structure of our quasi-solid gel enabled a high ratio of energy delivery with optimized ion transport channels with the aid of self-assembly of agarose which is stabilized by intra- and intermolecular hydrogen bonding. From a material design viewpoint, the gel can be deformed into various shapes and transferred to a conductive substrate, which is a scalable approach. Additionally, due to the low unit cost for agarose gel and NaCl components and the simple solution-mixing, heating, and casting methodology, this facile and cost effective characteristics assure convenient supercapacitor fabrication. In this regard, our tailored waterborne gel would be applied as a conducting media in flexible devices owing to its simple production with a high capacitance that matches that of a liquid electrolyte configuration. Furthermore, it is acceptable that NaCl and agarose are edible ensures eco-friendly nature of our fabricated gel electrolyte. It is believed that the quasi-solid gel would offer a convenient and green route to incorporating a high capacitance gel electrolyte in a supercapacitor permitting energy storage devices to be compatible for use in flexible electronics.

Chapter 2. Experiment

2.1 Preparation of electrodeposited MnO_2 thin film

As a substrate, an indium tin oxide-coated polyethylene terephthalate sheet (ITO-PET) was used for working electrode. The ITO-PET substrates (2 x 4 cm^2) were rinsed by ultrasonication in 1:1 mixture of iso-propanol and acetone ahead of the deposition. The electrodeposition was performed at room temperature using a WPG100 electrochemical workstation (WonAtech) with a three-electrode system. A Pt plate and Ag/AgCl were used as the counter electrode and reference electrode, respectively. Mn $(NO_3)_2$ (0.05 mol) and of $NaNO_3$ (0.075 mol) were dissolved in de-ionized (DI) water. The electrodeposition was performed potentiostatically at 1.0 V (vs. Ag/AgCl) under various electrodeposition time (100, 200 and 300s). After the electrodeposition, the as-synthesized films were rinsed with DI water and dried at room temperature for 24 h.

2.2 Preparation of quasi-solid electrolyte using an agarose gel

Various concentrations of 100 ml NaCl solutions (0.1, 0.25 and 0.5 mol) were prepared by mixing a NaCl solution (5 mol, Aldrich) and DI water followed by vigorous stirring. Subsequently, powdered agarose (1 g) was dissolved in the as-prepared NaCl solution (100 ml). The 1 % (w/v) agarose solution was heated using a microwave oven. After the agarose had completely dissolved, the solution was cast onto a glass plate and allowed to gel on the plate at room temperature for 15 min. Successively, the quasi-solid electrolyte derived from agarose gel was cut and separated (2 x 3 cm^2), and then assembled with MnO_2 electrodeposited ITO-PET electrode.

2.3 Characterization

The morphology and composition of electrodepositied MnO_2 films were characterized by scanning electron microscopy (SEM, Carl Zeiss., SUPRA 55VP), X-ray photoelectron spectroscopy (XPS, Thermo, K-Alpha), and X-ray diffraction (XRD, Rigaku, D/max-2200). Electrochemical characterization was performed using an assembled full cell with combination of the NaCl/agarose gel electrolyte with various NaCl concentrations (0.1, 0.25, and 0.5 M) and electrodeposited MnO_2 thin film electrode under two - electrode system. For the control group, 0.1 M NaCl solution was applied as for the liquid electrolyte within two - electrode configuration. Cyclic voltammetry (CV) and galvanostatic charge-discharge measurements were carried out using potentiostat (Iviumstat electrochemical analyzer, Ivium Technology) at potential window of 0 to 0.8 V, and various current densities (0.5 A g^{-1} to 10 A g^{-1}), respectively. Electrochemical Impedance Spectroscopy (EIS) was investigated using potentiostat (Iviumstat electrochemical analyzer, Ivium Technology) at various applied potentials (0.4 – 1.6 V). The AC amplitude was 10 mV and frequencies of 0.01 Hz to 100 kHz were used. Three quasi-solid type supercapacitors were assembled in series to drive red light-emitting diode (LED / 1.2 V, 20 mA) after charging each full cell for 30 s.

2.4 Calculation

The specific capacitances (F g^{-1}) of symmetrical supercapacitors are calculated in two ways as follows. Firstly, the specific capacitance was calculated using the cyclic voltammograms according to the equation (1):[50,51]

$$C = \frac{4 \times In_{CV}}{v \times \Delta V \times m} \quad (1)$$

where, In_{cv} is the area of integral for the discharged CV curve (AV), v is the sweep rate (mV s^{-1}), ΔV is the potential window (V) and m is the mass of the active material (g).

Secondly, the specific capacitance was calculated from the discharge curves of the galvanostatic charge-discharge results by equation (2):[52]

$$C = \frac{I \times \Delta t}{m \times \Delta V} \quad (2)$$

where I is the constant discharge current (A), Δt is discharging time (t), ΔV is the voltage (V) after the IR drop occurring at the discharging start point and m is the mass of the active material (g).

The energy density E, (W h kg^{-1}) at certain scan rate v (mV s^{-1}) was calculated based on equation (3):[53]

$$E = \frac{1}{2} \times C \times \Delta V^{2} \quad (3)$$

where the C is the value of specific capacitance (F g^{-1}) obtained by equation (1).

And the power density P, (W kg^{-1}) was calculated using the equation (4):[53]

$$P = \frac{E}{\Delta t} \quad (4)$$

where the E is the energy density (W h kg^{-1}) calculated by equation (3), and Δt is the discharging time (s).

Chapter 3. Results and discussion

3.1 Physical, chemical analysis of as-synthesized quasi-solid state supercapacitor

3.1.1 Synthesis procedure

The schematic design for assembling the supercapacitor with the quasi-solid agarose gel electrolyte and two electrodeposited MnO_2 electrodes is shown in Figure 3-1. More details of the synthesis process is described in the experimental section. Our method for assembling the supercapacitor with quasi-solid gel electrolyte has several merits, as below: First, this synthetic process is facile, non-toxic, and cost competitive for use in preparing quasi-solid-type supercapacitors as the gel electrolyte is fabricated through simple techniques such as solution-mixing, heating and casting in ambient conditions. Second, the size and thickness of the gel can be modified by utilizing razor blade and adjusting the number of the glass blocks used, as shown in Figure 3-2A. Furthermore, this interfacial gelation method is industrially feasible, since the gel can be transferred onto various substrates such as glass, stainless steel, and plastic plates and, with the help of the razor blade and glass blocks, the size and shape of the gel electrolyte can be easily varied as shown in Figure 3-2B. Third, by introducing the polymeric current collector which can provide flexible characteristics, the gelation-based assembly could be a promising method for the fabrication of larger flexible devices. As a synergetic effect of

these advantages, the introduction of an agarose gel as an electrolyte presents a simple way to produce quasi-solid-type supercapacitor by easily tuning its physical requirements.

3.1.2 Characterization of electrolyte and electrodes

3.1.2.1 NaCl/agarose gel electrolyte

As shown in Figure 3-3A, the as-synthesized NaCl/agarose-gel is transparent and thin, ensuring it suitable for exhibiting bendable and flexible characteristics. Cross-sectional SEM images of this gel were obtained after the freeze-drying process. These images verify that the gel is 3-dimensionally interconnected with an open porous structure, as shown in Figure 3-3B. The pore size of the gel appears a submicrometer scale in accordance with previously reported results [54, 55]. The reduction of pore size and volume compared to those of the gel itself is because of the sublimated volume of the water molecules, trapped in the inner pores before the freeze-drying process [56].

3.1.2.2 MnO_2 electrodes

In this report, a MnO_2 electrode was applied as a model electrode. The selection of MnO_2 as an electrode material is ascribed to factors like as producing complexity related with cost, natural abundance and eco-friendliness. It serves a role of evaluating the electrochemical properties of the assembled

supercapacitor and the changes in the configuration of the gel and liquid electrolyte. A full cell assembled with the quasi-solid agarose gel electrolyte and two MnO_2 electrodes are shown in Figure 3-3C. The MnO_2 was uniformly electrodeposited on the surface of the ITO-PET substrate as shown in Figure 3-3C, demonstrated by semi-transparent golden-color of the material [57]. The morphology of the electrodeposited MnO_2 was observed to be aligned vertically with the shape of irregular nanoflower, as shown in Figure 3-3D. These structures are the outgrowth of the electrodeposition process [58], and electrolytic ion mobility would be anticipated to enhance interconnected MnO_2 nanoparticles [59].

The crystalline properties of as-synthesized MnO_2, grown on the ITO-PET substrate, were examined for basal characterization of XRD, as shown in Figure 3-4. In case of MnO_2/ITO-PET and ITO-PET, no obvious peak differences were observed, which can be construded that the synthesized MnO_2 has an amorphous structure as previously reported [60], due to the absence of a heat treatment process.

Figure 3-5A and B respectively reveal XPS profiles of the Mn 2p and O 1s spectral region. The binding energies of Mn were observed 653.7 and 641.9 eV, respectively, which is in good accordance with the spin energy separation of previous reported results [61]. The binding energy of chemically bonded oxygen atoms within the MnO_2 were found to be 529.8, 531.1 and 532.5 eV, which are respectively assigned to be Mn-O-Mn for the tetravalent oxide, Mn-OH for the hydrated trivalent oxide and H-O-H bond for residual water, as shown in Figure 3-5B [62, 63]. In addition, the oxidation state can be calculated

using equation below where S denotes the peak intensity [63].

Oxidation state = 4S(Mn-O-Mn) – S(Mn-OH) + 3S(Mn-OH) / S(Mn-O-Mn)

Sequentially, the average valence of electrodeposited Mn within the MnO_2 is calculated to be +3.16 which is an intermediate oxidation state between Mn^{3+} and Mn^{4+}. These changes in oxidation state can be referred to charge storage mechanism of the redox reactions of amorphous MnO_2 as shown in equation below [63].

$$MnO_2 + xH^+ + yNa^+ + (x+y)e^- \leftrightarrow MnOOH_xNa_y$$

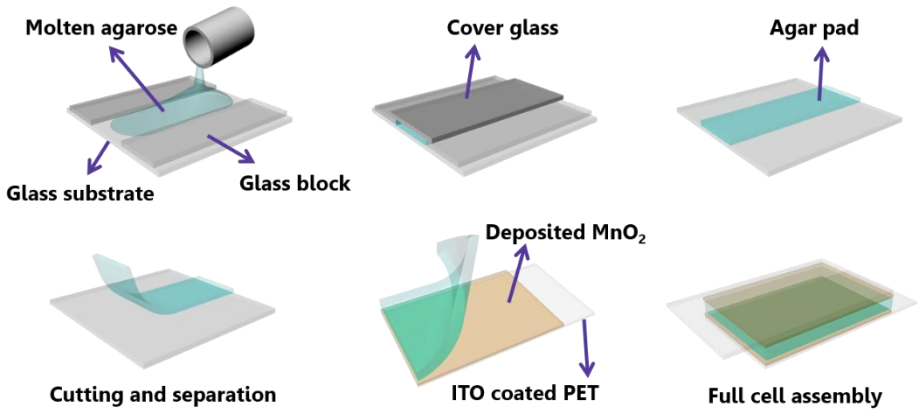

Figure 3-1. Schematic illustration displaying the formation of an agarose gel mediated MnO_2 symmetric cell assembly.

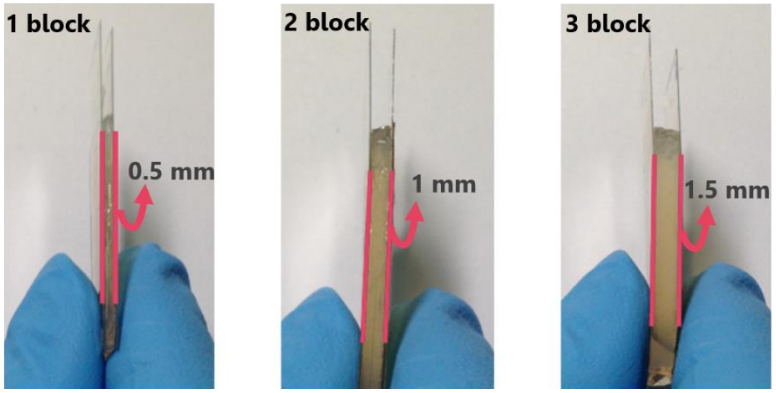

Figure 3-2A. Photographs of as-synthesized supercapacitors at varying depths of 1 block to 3 block.

Figure 3-2B. Shape adapted quasi-solid gel varying length and width into round, rectangular, and triangular form.

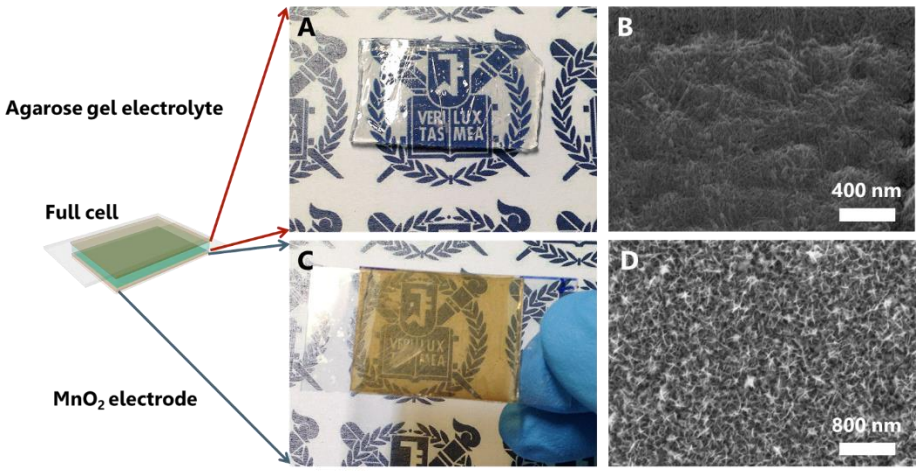

Figure 3-3. (A) Optical image and (B) SEM image of agarose gel. (C) Optical image and (D) SEM image of MnO_2 deposited ITO-PET.

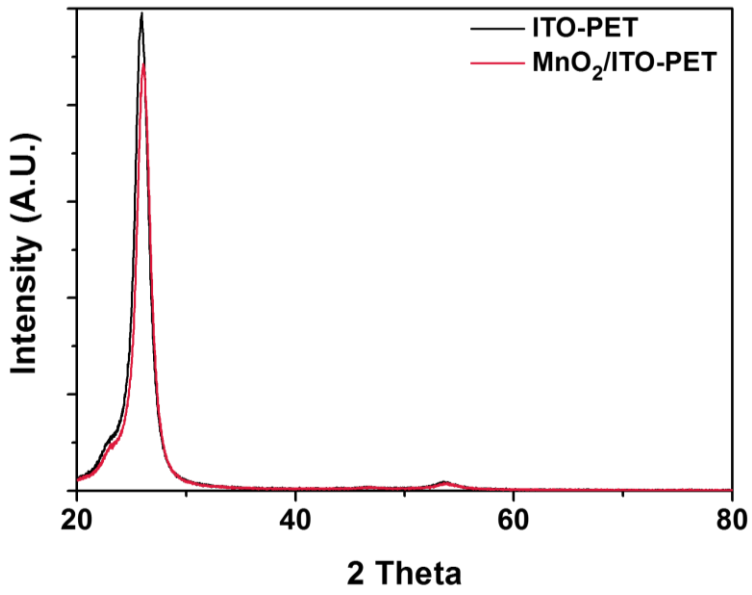

Figure 3-4. X-Ray diffraction patterns of ITO-PET and MnO_2/ITO-PET.

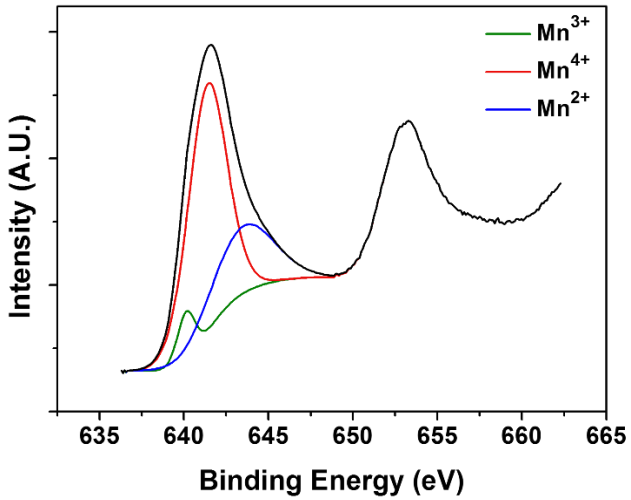

(A)

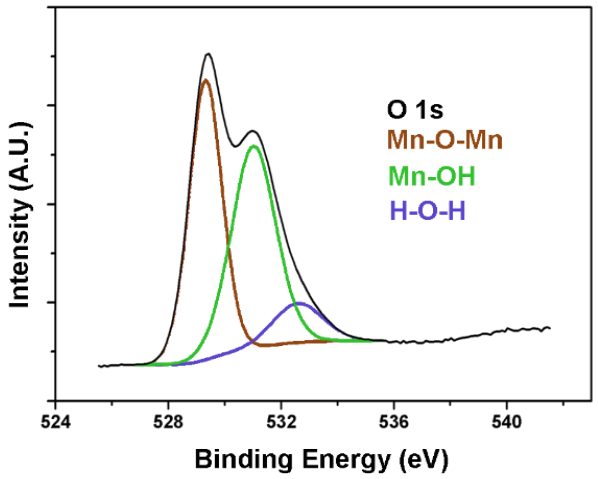

(B)

Figure 3-5. Results of an XPS analysis of MnO_2 coating layer for oxidation state determination, binding energies of **(A)** Mn 2p and **(B)** O 1s components.

3.2 Electrochemical performance

3.2.1 Optimization

In pursuance of optimizing the performance of the NaCl-agarose gel (denoted as NaCl-G), cyclic voltammetry (CVs) in different conditions were studied at a scan rate of 20 mV s^{-1}. Firstly, the dependency of CV performance on the thickness of the gel electrolyte was evaluated and the results are revealed in Figure 3-6. The CV curves were essentially the similar among gels with varied thickness from 1 (0.5 mm), 2 (1.0 mm) and 3 (1.5 mm) blocks adjusting overlapped glass plates, which indicates that the effects of electrolyte thickness on electrochemical performance are negligible. Therefore, the minimum thickness of 1 block gel electrolyte, was employed as a criterion thickness for charge storage with high ion conductivity and for securing the required flexibility in this report. Secondly, the shapes of all of the CV curves with NaCl concentrations from 0.1 to 0.5 M (Figure 3-7) were also analogous to one another. Since the total area of the substrate electrodeposited with MnO_2 is constant, net amount of ions that can be inserted or detached at the surface of the electrode is surmised to be constant as well. Thus, it can be concluded 0.1 M is a sufficient concentration to activate the surface of the electrode. 0.1 M was used as the standard concentration for NaCl-G. Figure 3-8 shows the CV profiles for varying deposition times for MnO_2 synthesis ranging 100, 200, and 300 seconds. The results indicate that a sample with a deposition time of 200 seconds exhibited the highest current density among all the samples tested. The

relatively low amount of electrodeposited MnO_2 for 100 seconds was not sufficient for achieving ample specific capacitances, and a condensed packing on the sample of 300 seconds electrodeposition leads to a surface area of MnO_2 cannot be fully utilized [64]. Hence, the 200 seconds was chosen for MnO_2 optimum electrodeposition time.

3.2.2 Cyclic voltammetry measurement

Figure 3-9A and B show the CV results from the supercapacitors with the NaCl-G and 0.1 M NaCl aqueous solution (NaCl-L), respectively. For this comparison, NaCl-G was fabricated in terms of 0.5 mm thickness (thickness of one glass plate), and 0.1 M NaCl concentration was taken due to the negligible effects of gel thickness and NaCl concentration on electrochemical performance, on the basis of the above mentioned investigation. On the both NaCl-G and NaCl-L configuration, CV profiles showed similar quasi-rectangular and symmetrical shapes, indicating the rate capability for NaCl-G is comparable to that for NaCl-L. Moreover, similar shapes and current densities for CV curves from both electrolytes at same scan rates imply that the supercapacitive behavior of the NaCl-G is not impeded because of the excellent ion conductivity, which is analogous to the NaCl-L. At the smallest scan rate of 5 mV s^{-1}, the specific capacitance calculated from the CVs for NaCl-G was 200 F g^{-1}, which is comparable to that for NaCl-L (209 F g^{-1}). Furthermore, the specific capacitance of the supercapacitor with NaCl-G was 80 % of that for the NaCl-L at higher scan rate, 100 mV s^{-1}, which infers that the performance

of the NaCl-G would be similar to that of NaCl-L.

3.2.3 Comparison of electrochemical performance

The normalized specific capacitances of the full cell with NaCl-G and NaCl-L were plotted as a function of scan rates, with the standard of specific capacitance of 5 mV s^{-1} as shown in Figure 3-10. It has been reported that the specific power of a supercapacitor is highly affected by the ion movement in the full cell [65]. Accordingly, a supercapacitor with NaCl-G performed a comparable rate capability to that of NaCl-L. With increase of scan rate, the decreases in specific capacitance for both electrolyte configuration are due to the increase of charge resistance of the material [66]. Moreover, the similar degree of decrease for both electrolytes within the measured range of scan rates verifies that the ion mobility in the NaCl-G is sufficiently analogous to compete with NaCl-L [29].

Electrochemical impedance spectroscopy was performed for examining the resistivity behaviors of the supercapacitors fabricated by NaCl-G and NaCl-L, as shown in Figure 3-11. The impedance results for NaCl-G (318.1 Ω) showed a higher value of ESR of the electrode material (an intercept on the real axis in the high frequency region) than that of NaCl-L (139.1 Ω). This would be estimated, because the charge transfer for NaCl-G features a relatively high contact resistance between the quasi-solid gel and electrode than that for NaCl-L caused by a liquid phase electrolyte based ion mobility. The higher contact loss contributes to a reduction in specific capacitances, which is in good

agreement with the relatively lower specific capacitances for NaCl-G compared to that for NaCl-L. The semicircular behavior at the high- to middle-frequency region related to the interfacial resistance between electrode material and electrolyte, showed matchable values (~ 20.9 Ω) under both electrolyte configurations. This arises from the same redox reaction between electrolyte ions and the MnO_2 involved in both electrolytes. It was also confirmed that the supercapacitors with both electrolytes are not involved in Warburg impedance, which denote the diffusivity of the electrolyte ions, on the basis of the fact that there is no line that intersects the real axis near an angle of 45 °[26]. The slope of the NaCl-L plot is similar to that for the NaCl-G, indicating comparable power characteristic of the developed gel system and the conventional liquid system. The power characteristics of the configurations can also be compared by a Ragone plot. Figure 3-12 displays the Ragone plot obtained from the total mass of active materials for both the positive and the negative electrodes of NaCl-G and NaCl-L. The curves from both NaCl-G and NaCl-L showed a similar magnitude and variation tendency.

3.2.4 Charge/discharge measurement

The charge and discharge profile of the supercapacitor with NaCl-G was investigated at current density range of 0.5 to 10 A g^{-1} by using the symmetric two-electrode system shown in Figure 3-13. These galvanostatic curves displayed triangular forms with a small internal resistance (IR) drop in a measured range of current densities, which imply excellent rate capability [67].

The specific capacitances for NaCl-G, evaluated from the discharge time, were calculated to be 286.9 and 268.1 F g^{-1} at a current density of 0.5 and 1 A g^{-1}, respectively, which are similar or prior to previously reported capacitance values for MnO_2 - gel electrolyte based supercapacitors, as shown in Table 1.

3.2.5 Functional mechanism of NaCl/agarose-gel

The supercapacitive behavior of the NaCl-G supercapacitor as a quasi-solid-state full-cell can be ascribed to the porous structure of NaCl-G, which offers various merits for ion transport. According to the charge storage mechanism, MnO_2 can perform a faradaic reaction in a sodium based electrolyte system [71]. The diffusivity and rate of insertion (or extraction) of participating protons and sodium ions in the redox reaction can act as effective parameters for determining the rate capability. In this regard, diffusivity can be improved by an intimate contact between the MnO_2 and electrolyte as well as a low resistance to diffusion by introducing an interconnected porous system, which could also enhance the ionic adsorption of electrolyte ions onto the surface of the MnO_2. In that respect, our quasi-solid gel could effectively improve power density by offering 3D channel networks filled with an electrolyte in an aqueous medium. Here, we propose the illustrative cross section structure of NaCl-G as shown in Figure 3-14. An agarose hydrogel is composed of a chemically interconnected agarose backbone and oriented inter-particular submicropores filled with water molecules (Figure 3-14), formed by a hydrogen-bonded crosslinking self-assembly mechanism (Figure 3-15). The gel is positioned

between the positive and negative electrodes, which plays role of preventing physical contact of the electrodes, and supporting free ionic transport with a perfect isolation of electronic flow [72]. The functional betterment of NaCl-G can be attributed to three factors. Firstly, the agarose matrix retains mechanical properties of the gel as a framework. As shown in Figure 3-15, the hydrogen bonding between the agarose polymers simultaneously reinforce the 3D network formation and improve mechanical stability. Secondly, the submicropores with the water filler offer an ion reservoir, hence providing an ionic pathway to the storage sites of MnO_2 [73]. Apparently, ionic conductance can be easily improved within the agarose hydrogel by enveloping the aqueous ionic liquid [46, 74]. Lowering the viscosity of the electrolyte introducing water filler facilitates the development of moist pore networks, which plays a significant part of ion conducting channels as shown in Figure 3-15 [75]. The accessibility of ions in the pore networks highly relies on the sizes of the pores and the type of electrolyte ions [73]. The inner diameters of the pores in the quasi-solid gel, which approximate on a submicrometer scale, would be sufficient to accommodate the sodium and chloride ions. The wide application of the agarose gel in DNA (bigger than Na^+ or Cl^-) electrophoresis supports this deduction [76]. Thirdly, the introduction of sodium chloride to a quasi-solid gel as an ionic liquid is also beneficial in terms of enhancing ionic conductivity. This is because Na^+ can prohibit electrode polarization, which can be caused by an increase in H^+ originating from the electrolysis of water as the result of overcharging and overdischarging [46]. The ionic conductance of Na^+ can also be improved by the synergetic effect with negatively charged functionalities on

the agarose backbone such as sulfate, pyruvate, glucuronate and others [46]. Subsequently, the hierarchical pore structure of the NaCl-G provide open spaces facilitating the accessibility of electrolyte ions, which offers enhanced utilization of 3-dimensionally located electrolyte ions within the pores [43]. Following on this, an improved interfacial contact would provide electrochemical reciprocity for the quasi-solid gel.

3.2.6 Flexibility, stability, and practical application

For verifying the flexible nature of the NaCl-G, we devised a one-planar interdigitated prototype supercapacitor. MnO_2 was electrodeposited in one planar configuration with a partition for arraying the cathode and anode, which is depicted in the inset of Figure 3-16A, B, and C. When the NaCl-G supercapacitor is bent with a bending radius of 1.16 cm, no significant variance in the CV curves was observed in three different bending status; when it is flat (Figure 3-16A), as the form of compressive bending (in-plane conformation, Figure 3-16B), and of tensile bending (out-of-plane conformation, Figure 3-16C) and the collective profile is shown on 3-17A. Electrochemical impedance measurements were performed in order to observe the resistive behaviors of the fabricated supercapacitor under aforesaid bending conditions, as shown in Figure 3-17B. Nyquist plots exhibited almost equal semicircular behavior (~ 496.5 Ω) under the three arrangements, suggesting that comparable charge transfer rate with three different bending status. Based on the results, the NaCl-G is very stable under various bending conditions, indicating the resultant full-

cell is suitable for flexible device applications.

The stability of the NaCl-G-supercapacitors was investigated by CVs at a scan rate of 100 mV s^{-1}. The specific capacitance variation as a function of cycle number is shown in Figure 3-18A. During the retention test, the full cell of MnO_2/NaCl-G/MnO_2 configuration was thoroughly sealed by PTFE sealant tape and sticky polypropylene tape as shown in Figure 3-18A inset. The normalized specific capacitances (the specific capacitances divided by the value of tenth cycle) begin to reduce after 600 cycles and approximately 80% of the maximum capacity is retained after 1200 cycles. The enveloped cell exhibited better cycle stability compared to the the non-enveloped cell which showed 34 % capacity retention. The relatively enhanced durability with the sealed cell is consistent with the cycle stability of previously reported MnO_2 based supercapacitors [77, 78]. This enhancement can be considerably attributed to the retention of interconnected wet ion transfer pore channels, with appropriate sealing which prevents the evaporation of water. This suggests that the stability of a NaCl-G based supercapacitor could be improved with an enhancement in sealing process for commercialization. In addition, it was demonstrated that the assembled full cell device can activate a red light emitting diode (Figure 3-18B).

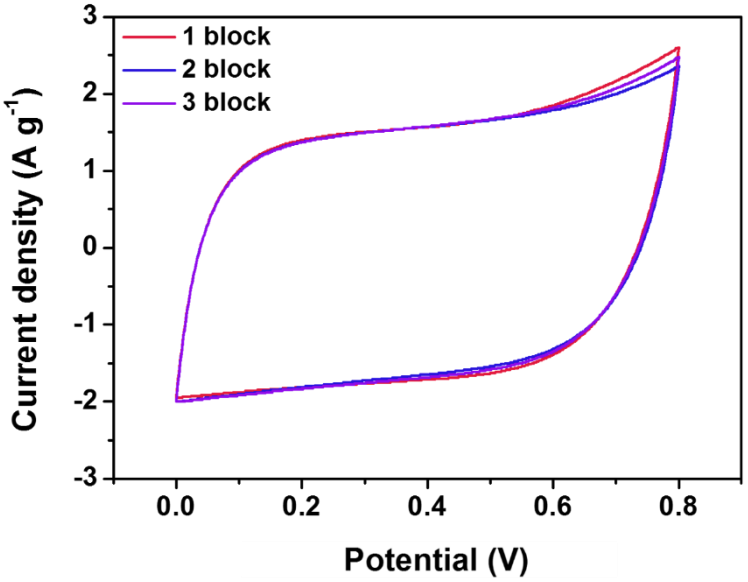

Figure 3-6. Comparative cyclic voltammetry profile with variation of gel electrolyte thickness

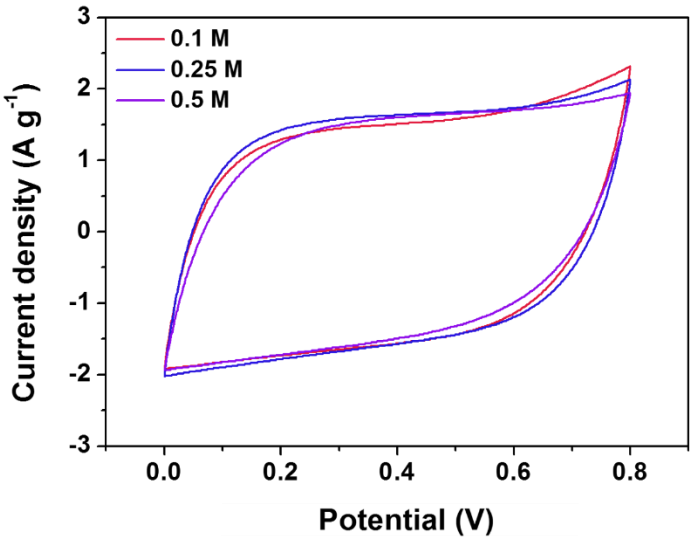

Figure 3-7. Comparative cyclic voltammetry profile with variation of NaCl concentration in gel electrolyte

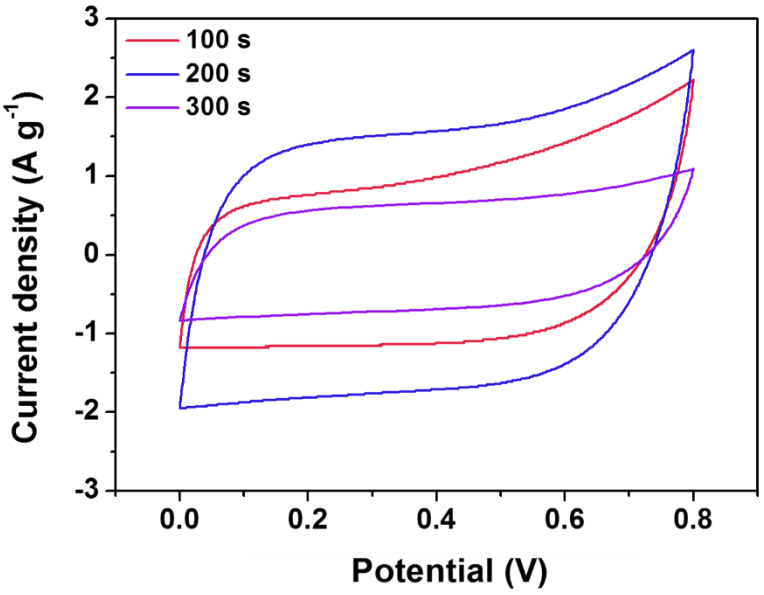

Figure 3-8. Comparative cyclic voltammetry profile with variation of MnO_2 electrodeposition time.

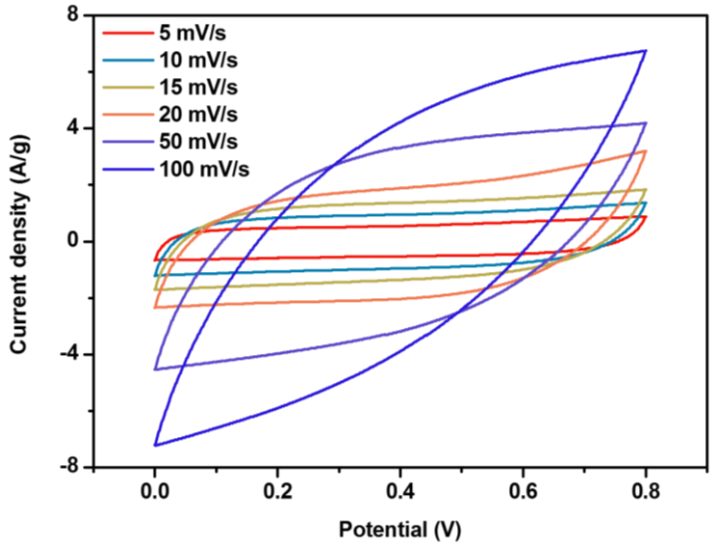

(A)

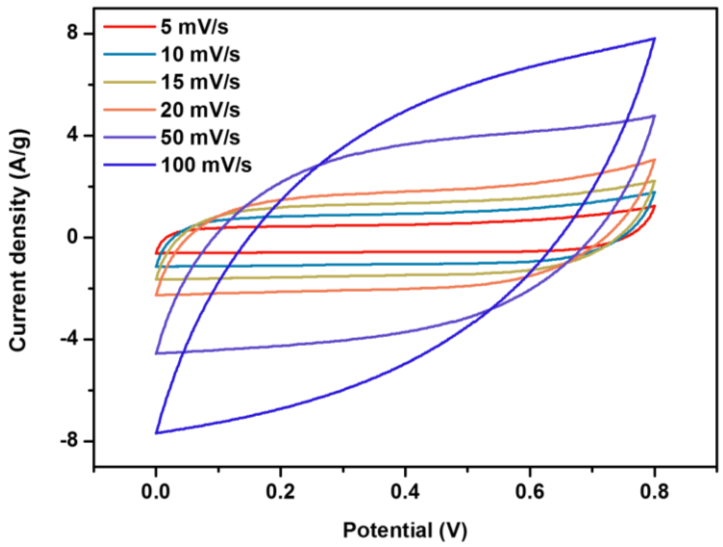

(B)

Figure 3-9. CVs for (A) NaCl-G, (B) NaCl-L over a range of 5-100 mV s^{-1}

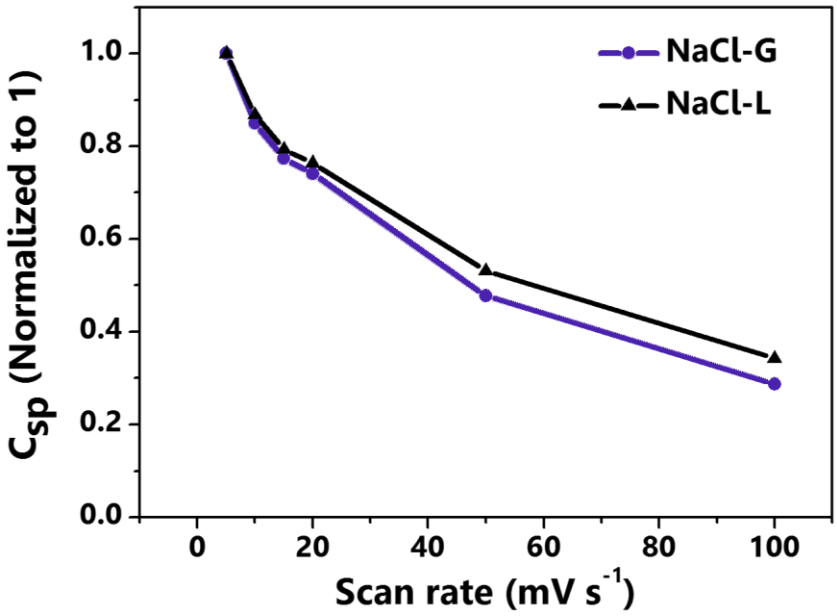

Figure 3-10. Normalized specific capacitance of NaCl-G and NaCl-L at scan rate of 5-100 mV^{-1}.

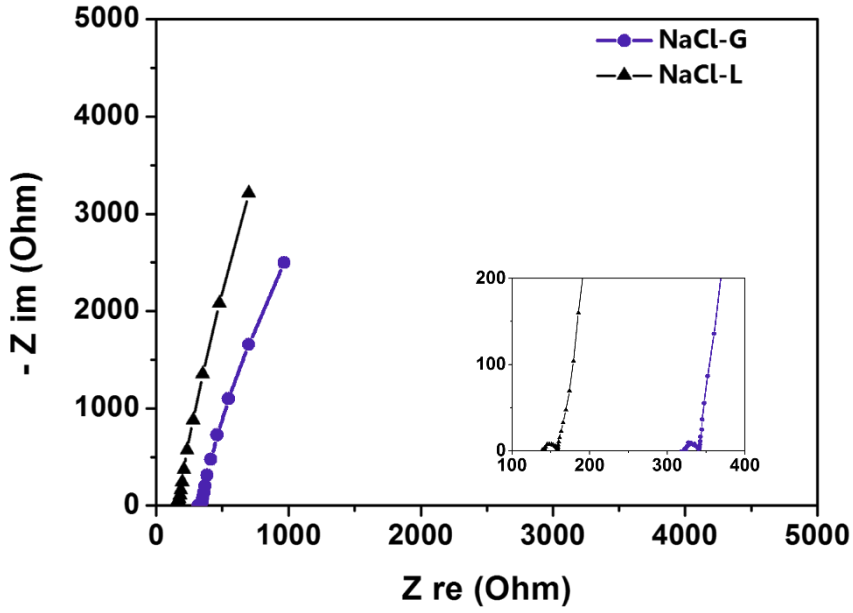

Figure 3-11. The Nyquist impedance plot of NaCl-G and NaCl-L.

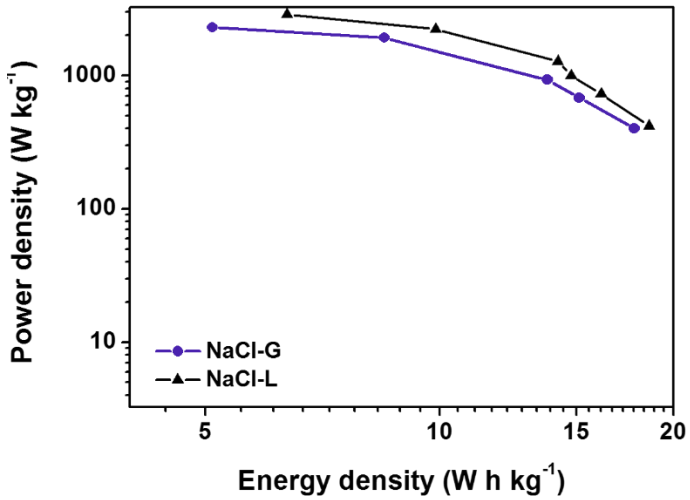

Figure 3-12. The Ragone plot of NaCl-G and NaCl-L.

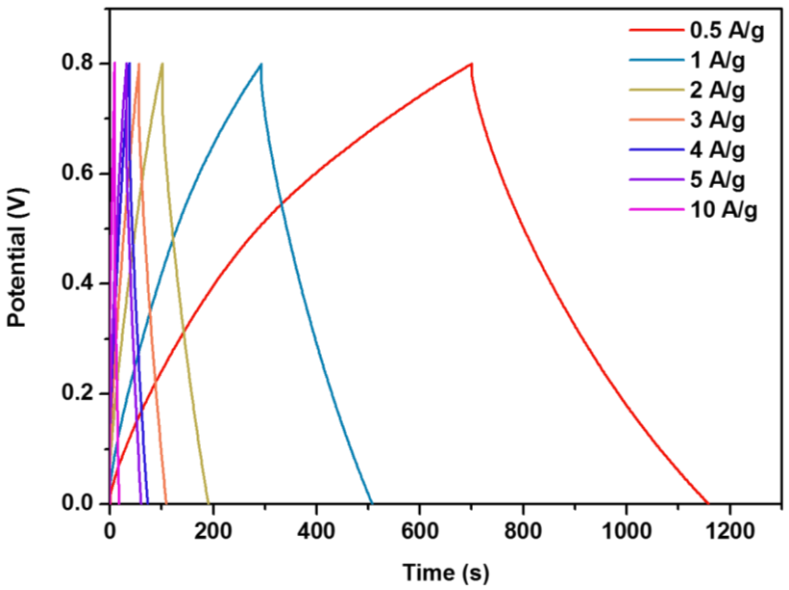

Figure 3-13. The Charge/discharge profile of NaCl-G.

Materials	Electrolytes	Capacitances [F g^{-1}]	Ref.
MnO_2	PVA/H_3PO_4	335 (at 10 mV s^{-1})	[59]
CNT/CNO- MnO_2	[EMIM][NTf_2]-PVdF(HFP)	138 (at 2 mV s^{-1})	[68]
MnO_2	Na_2SO_4 + 3 wt% SiO_2	150 (at 100 mV s^{-1})	[69]
MnO_2/Graphene	PVA/H_3PO_4	254 (at 0.5 A g^{-1})	[70]
MnO_2	Agarose/NaCl gel	286.1 (at 0.5 A g^{-1})	This Work

Table 1. Comparison of previously reported specific capacitance data for MnO_2 based supercapacitors with our work.

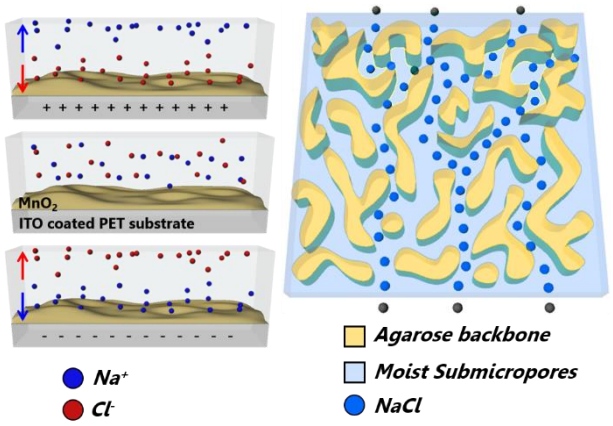

Figure 3-14. The proposed schematic design of ion transport in the agarose gel.

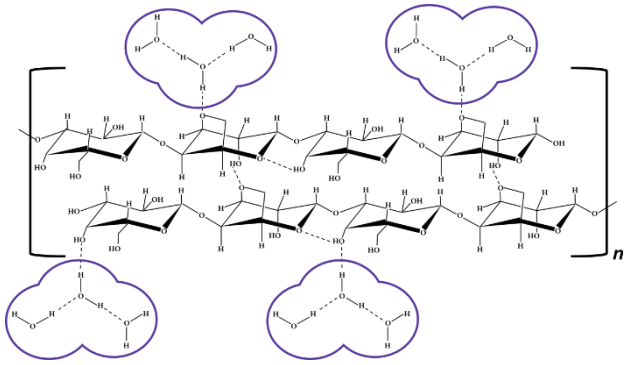

Figure 3-15. The scheme of the synthesis of an agarose gel.

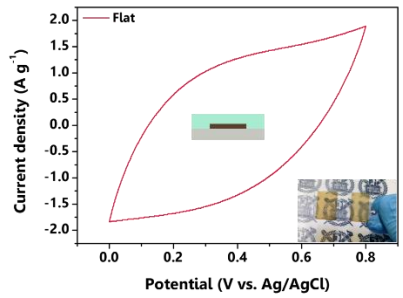

(A)

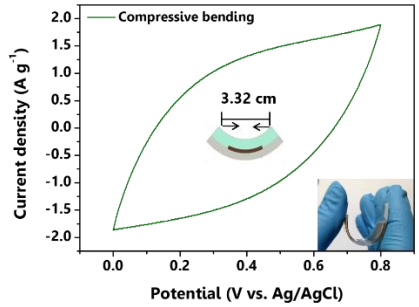

(B)

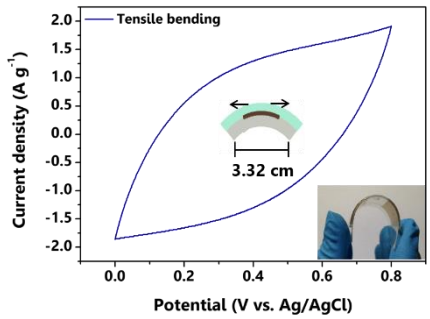

(C)

Figure 3-16. Comparing CV profile of as-synthesized sample with digital photo of 3 different bending status; (A) flat, (B) compressive bending, (C) tensile bending.

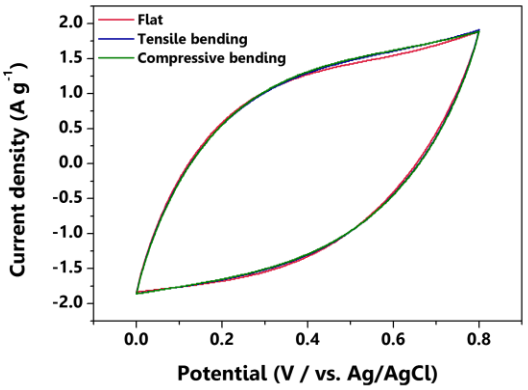

(A)

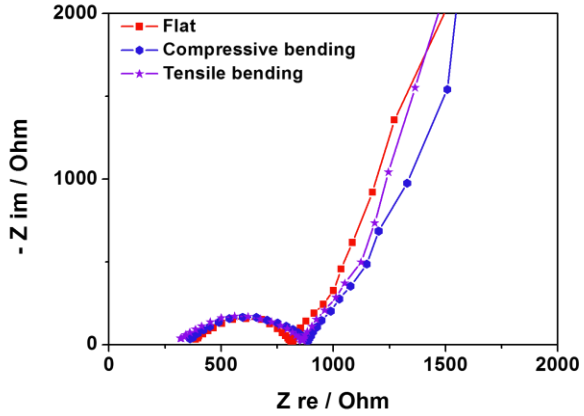

(B)

Figure 3-17. Collective (A) CV, (B) EIS profile of as-synthesized sample with digital photo of 3 different bending status.

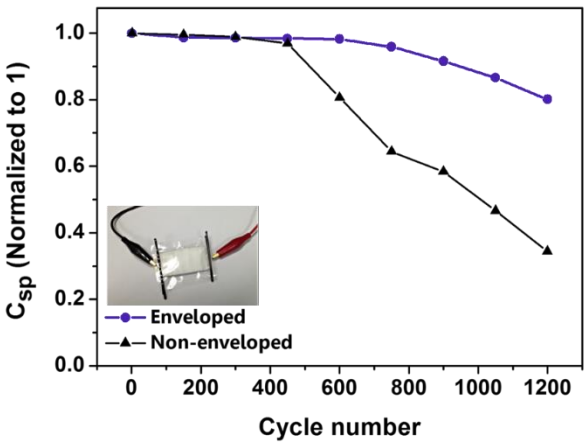

(A)

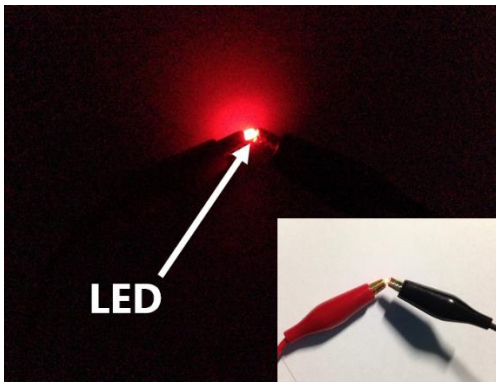

(B)

Figure 3-18. (A) The stability test profile of sealed and unsealed NaCl-G supercapacitors, (B) digital photo of a light-emitting diode (LED) activated by the NaCl-G supercapacitors.

Chapter 4. Summary and Conclusions

In summary, this dissertation report on an agarose/NaCl quasi-solid gel for use as a supercapacitor electrolyte material. Our quasi-solid gel electrolyte has several merits, firstly, synthesis of the gel electrolyte is simple at low-cost, and scalable which is plausible for mass production. Additionally, in terms of handling, the shape of the gel can easily be modified by using plain gadgets, and the gel can be transferred onto most of substrates, indicating the use of such gel is industrially feasible. Inclusively, flexible supercapacitor can be assembled by introducing the polymeric current collector with our gel, assuring the gelation-based full cell build-up of a promising method for the fabrication of larger flexible devices. Secondly, supercapacitor assemble with our gel exhibited high electrochemical performance that matches that of a liquid electrolyte configuration. On account of the 3D hierarchical porous network as an optimized ion transport channel in the gel, the fabricated gel electrolyte performed high specific capacitances and rate capability. Furthermore, agarose-NaCl combination introduced in the gel electrolyte features culinary characteristics which ensures the safe fabrication and applications with biodegradability. Thus, we believe that our quasi-solid gel electrolyte would offer attractive prospects and could be extended to further application with its high performance, simplicity of fabrication and eco-friendly properties.

References

[1] Winter, M., Brodd, R. J., *Chem. Rev.*, **104** (2004), 4245.

[2] Hall, P. J., Mirzaeian, M., Fletcher, S. I., Sillars, F. B., Rennie, A. J. R., Shitta-Bey, G. O., Wilson, G., Cruden, A., Carter, R., **3** (2010), 1238.

[3] Wang, G. P., Zhang, L., Zhang, J. J., *Chem. Soc. Rev.*, **41** (2012), 797.

[4] A. Lewandowski, M. Galinski, *J. Power Sources*, **173** (2007), 822.

[5] O. Bohlen, J. Kowal, D.U. Sauer, *J. Power Sources*, **172** (2007), 468.

[6] B. E. Conway, *Electrochemical Supercapacitors*, Kluwer Academic/Plenum Press, New York, 1999.

[7] B. Babakhani, D. G. Ivey, *Electrochim. Acta*, **55** (2010), 4014.

[8] S. Sarangapani, B. V. Tilak, C. P. Chen, *J. Electrochem. Soc.*, **143** (1996), 3791.

[9] M. S. Wu, P. C. Chiang, *Electrochem. Solid-State Lett.*, **7** (2004), A123.

[10] W. Sugimoto, H. Iwata, Y. Murakami, Y. Takasu, *J. Electrochem. Soc.*, **151** (2004), A1181.

[11] X. Dong, W. Shen, J. Gu, L. Xiong, Y. Zhu, H. Li, J. Shi, *J. Phys. Chem. B*, **110** (2006), 6015.

[12] V. V. N. Obreja, *Physica E*, **40** (2008), 2596.

[13] M. Inagaki, H. Konno, O. Tanaike, *J. Power Sources*, **195** (2010), 7880.

[14] A. Burke, *J. Power Sources*, **91** (2000), 37.

[15] R. Kötz, M. Carlen, *Electrochim. Acta*, **45** (2000), 2483.

[16] Y. Zhang, H. Feng, X. Wu, L. Wang, A. Zhang, T. Xia, H. Dong, X. Li, L. Zhang, *Int. J. Hydrogen Energy*, **34** (2009), 4889.

[17] H. Chen, T. N. Cong, W. Yang, C. Tan, Y. Li, Y. Ding, *Prog. Nat. Sci.*, **19**

(2009), 291.

[18] R. N. Reddy, R. G. Reddy, *J. Power Sources*, **132** (2004), 315.

[19] B. Babakhani, D. G. Ivey, *J. Power Sources*, **195** (2010), 2110.

[20] J. Lee, K. Liang, K. An, Y. Lee, *Synth. Met.*, **150** (2005), 153.

[21] Anothumakkool, B., Torris, A. A. T., Bhange, S. N., Badiger, M. V., Kurungot, S., *Nanoscale*, **6** (2014), 5944.

[22] Li, L., Wu, Z., Yuan, S., Zhang, X.-B., *Energy Environ. Sci.*, **7** (2014), 2101.

[23] Niu, Z., Dong, H., Zhu, B., Li, J., Hng, H. H., Zhou, W., Chen, X.; Xie, S., *Adv. Mater.*, **25** (2013), 1058.

[24] Henderson, W. A., Brooks, N. R., Young, V. G., Jr., *J. Am. Chem. Soc.*, **125** (2003), 12098.

[25] Quartarone, E., Mustarelli, P., *Chem. Soc. Rev.*, **40** (2011), 2525.

[26] Yang, X., Zhang, F., Zhang, L., Zhang, T., Huang, Y., Chen, Y., *Adv. Funct. Mater.*, **23** (2013), 3353.

[27] Croce, F., Appetecchi, G. B., Persi, L., Scrosati, B., *Nature*, **394** (1998), 456.

[28] Kawasaki, M., Iwasa, Y., *Nature*, **489** (2012), 510.

[29] Lodge, T. P., *Science*, **321** (2008), 50.

[30] Niu, Z., Zhang, L., Liu, L., Zhu, B., Dong, H., Chen, X., *Adv. Mater.*, **25** (2013), 4035.

[31] Ding, X., Zhao, Y., Hu, C., Hu, Y., Dong, Z., Chen, N., Zhang, Z., Qu, L., *J. Mater. Chem. A*, **2** (2014), 12355.

[32] Wang, G., Lu, X., Ling, Y., Zhai, T., Wang, H., Tong, Y., Li, Y., *ACS Nano*, **6** (2012), 10296.

[33] Huang, C. W., Wu, C. A., Hou, S. S., Kuo, P. L., Hsieh, C. T., Teng, H.,

Adv. Funct. Mater., **22** (2012), 4677.

[34] Lee, J., Panzer, M. J., He, Y., Lodge, T. P., Frisbie, C. D., *J. Am. Chem. Soc.*, **129** (2007), 4532.

[35] Sampath, S., Shin, W. H., Choi, J. W., Coskun, A., *J. Mater. Chem. A*, **1** (2013), 43.

[36] Tako, M., Nakamura, S., *Carbohydr. Res.*, **180** (1988), 277.

[37] Kim, G.-P., Park, S., Nam, I., Park, J., Yi, J., *J. Mater. Chem. A*, **1** (2013), 3872 .

[38] Ross, K. A., Scanlon, M. G., **30** (1999), 17.

[39] Normand, V., Lootens, D. L., Amici, E., Plucknett, K. P., Aymard, P., *Biomacromolecules*, **1** (2000), 730.

[40] Duffus, C., Camp, P. J., Alexander, A. J., *J. Am. Chem. Soc.*, **131** (2009), 11676.

[41] Clar, J. G., Silvera Batista, C. A., Youn, S., Bonzongo, J. C., Ziegler, K. J., *J. Am. Chem. Soc.*, **135** (2013), 17758.

[42] Wang, X., Egan, C. E., Zhou, M. F., Prince, K., Mitchell, D. R. G., Caruso, R. A., *Chem. Commun.*, 2007, 3060.

[43] Koo, H.-J., Chang, S. T., Slocik, J. M., Naik, R. R., Velev, O. D., *J. Mater. Chem.*, **21** (2011), 72.

[44] Singh, T., Trivedi, T. J., Kumar, A., *Green Chem.*, **12** (2010), 1029.

[45] S. Lu., *Sci. Rep.*, **4** (2014), 5464.

[46] Koo, H.-J., Chang, S. T., Velev, O. D., *Small*, **26** (2010), 1393.

[47] Koo, H.-J., So, J.-H., Dickey, M. D., Velev, O. D., *Adv. Mater.*, **23** (2011), 3559.

[48] Cayre, O. J., Chang, S. T., Velev, O. D., *J. Am. Chem. Soc.*, **129** (2007), 10801.

[49] Mandal, L., Deo, M., Yengantiwar, A., Banpurkar, A., Jog, J., Ogale, S., *Adv. Mater.*, **24** (2012), 3686.

[50] Ji, J., Zhang, L. L., Ji, H., Li, Y., Zhao, X., Bai, X., Fan, X., Zhang, F., Ruoff, R. S., *ACS Nano*, **7** (2013), *7*, 6237.

[51] Kim, T., Jung, G., Yoo, S., Suh, K. S., Ruoff, R. S., *ACS Nano*, **7** (2013), 6899.

[52] Lei, Z., Shi, F., Lu, L., *ACS Appl. Mater. Interfaces*, **4** (2012), 1058.

[53] Zhang, C., Peng, Z., Lin, J., Zhu, Y., Ruan, G., Hwang, C. C., Lu, W., Hauge, R. H., Tour, J. M., *ACS Nano*, **7** (2013), 5151.

[54] Pernodet, N., Maaloum, M., Tinland, B., *Electrophoresis*, **18** (1997), 55.

[55] Pluen, A., Netti, P. A., Jain, R. K., Berk, D. A., *Biophys. J.*, **77** (1999), 542.

[56] Maiti, U. N., Lim, J. W., Lee, K. E., Lee, W. J., Kim, S. O., *Adv. Mater.*, **26** (2014), 615.

[57] Liu, D., Zhang, Q., Xiao, P., Garcia, B. B., Guo, Q., Champion, R., Cao, G., *Chem. Mater.*, **20** (2008), 1376.

[58] Chen, W., Rakhi, R. B., Hu, L. B., Xie, X., Cui, Y., Alshareef, H. N., *Nano Lett.*, **11** (2011), 5165.

[59] Nam, I., Park, S., Kim, G.-P., Park, J., Yi, J., *Chem. Sci.*, **4** (2013), 1663.

[60] Xia, H., Zhu, D., Luo, Z., Yu, Y., Shi, X. Q., Yuan, G. L., Xie, J. P., *Sci. Rep.*, **3** (2013), 2978.

[61] Sumboja, A., Foo, C. Y., Wang, X., Lee, P. S., *Adv. Mater.*, **25** (2013), 2809.

[62] Rakhi, R. B., Chen, W., Cha, D., Alshareef, H. N., *Adv. Energy Mater.*, **2** (2012), 381.

[63] Toupin, M., Brousse, T., B ́danger, D., *Chem. Mater.*, **16** (2004), 3184.

[64] Yu, Z., Thomas, J., *Adv. Mater.*, **26** (2014), 4279.

[65] Korenblit, Y., Rose, M., Kockrick, E., Borchardt, L., Kvit, A., Kaskel, S., Yushin, G., *ACS Nano*, **4** (2010), 1337.

[66] Xu, Y., Lin, Z., Huang, X., Liu, Y., Duan, X., *ACS Nano*, **7** (2013), 4042.

[67] Yu, H., Zhang, Q., Joo, J. B., Li, N., Moon, G. D., Tao, S., Wang, L., Yin, Y., *J. Mater. Chem. A*, **1** (2013), 12198.

[68] Gao, Y., Zhou, Y. S., Qian, M., Li, H. M., Redepenning, J., Fan, L. S., He, X. N., Xiong, W., Huang, X., Majhouri-Samani, M., Jiang, L., Lu, Y. F., *RSC Adv.*, **3** (2013), 20613.

[69] Nam, H.-S., Kwon, J. S., Kim, K. M., Ko, J. M., Kim, J.-D., *Electrochim. Acta*, **55** (2010), 7443.

[70] Peng, L. L., Peng, X., Liu, B. R., Wu, C. Z., Xie, Y., Yu, G. H., *Nano Lett.*, **13** (2013), 2151.

[71] Mai, L., Li, H., Zhao, Y., Xu, L., Xu, X., Luo, Y., Zhang, Z., Ke, W., Niu, C., Zhang, Q., *Sci. Rep.*, **3** (2013), 1718.

[72] Hong, S. B., Park, S. H., Kim, J.-H., Lee, S.-Y., Kwon, Y. S., Park, T., Kang, P.-H., Hong, S. C., *Adv. Energy Mater.*, **4** (2014), , 1400477.

[73] Zeller, M., Lorrmann, V., Reichenauer, G., Wiener, M., Pflaum, J., *Adv. Energy Mater.*, **2** (2012), 598.

[74] Trivedi, T. J., Rao, K. S., Kumar, A., *Green Chem.*, **16** (2014), 320.

[75] Liu, X., Wu, D., Wang, H., Wang, Q., *Adv. Mater.*, **26** (2014), 4370.

[76] Chu, H. S., Choi, C. Y., Won, J. I., *Korean J. Chem. Eng.*, **25 (**2008), 1125.

[77] Chen, S., Zhu, J., Wu, X., Han, Q., Wang, X., *ACS Nano*, **4** (2010), 2822.

[78] Zhang, Z. S., Zhai, T., Lu, X. H., Yu, M. H., Tong, Y. X., Mai, K. C., *J. Mater. Chem. A*, **1** (2013), 505.

국 문 초 록

에너지저장장치 (Energy storage devices, ESD) 의 일환으로써, 슈퍼커패시터는 빠른 충, 방전 속도와 긴 수명 그리고 친환경성으로 주목을 받아왔다. 슈퍼커패시터의 에너지와 출력 밀도를 아우르는 성능 향상을 도모하기 위해 구성성분인 전극과 전해질의 개선이 선행되어야 한다. 특히, 전해질은 음극과 양극을 연결하여 이온의 수송을 담당하는 매개이자 슈퍼커패시터의 변형성을 가늠하는 중요한 요소로 작용한다. 따라서, 전해질의 형태에 대한 연구는 변형가능하고 소형화된 전력 공급 장치 개발을 목표로 하는 근래의 연구 트렌드와 궤를 함께 하여 응용의 확장성에 기여할 수 있을 것으로 예상된다. 고로, 높은 성능을 발현하고 쉽게 모양을 변형할 수 있으며 낮은 증기압과 가연성 물질을 활용하지 않고 상온에서 용이하게 합성이 가능한 전해질 개발이 요구된다.

한천 겔은 수분을 함유하고 있어 변형이 가능하며 높은 탄력성을 지녔고 친환경적이며 저렴한 단가로 제조할 수 있다는 장점을 갖고 있다. 겔의 내부에는 수분을 포함한 상호 연결된 다공성 구조가 최적화된 통로 역할을 하여 전기장 내에서 DNA, 단백질, 이온들 같은 대전된 입자들의 확산을 촉진하는 역할을 한다. 이런 현상을 바탕으로, 식품 생산, 생물학 연구와 더불어 한천은 그것을

기반으로 한 다양한 전자장비 합성에 응용된다. 그러나 한천 겔을 슈퍼커패시터 전해질로의 실용적, 실질적 적용에 대해서는 아직까지 보고된 바가 없다. 본 논문에서는 이산화망간 전극과 한천-염화나트륨 겔 전해질을 조합한 슈퍼커패시터를 합성하여 특성 분석을 수행한 내용을 수록하고 있으며, 간편한 합성 공정에 기반하여 고성능 플렉시블 슈퍼커패시터 구현을 위해 전극과 전해질의 최적 합성 조건을 분석하였다.

연구 결과로부터 한천-염화나트륨 겔을 슈퍼커패시터를 응용하는 것이 몇 가지 주목할 만한 장점을 가진다는 것을 파악하였다: (1) 겔의 합성과정 중 용액 혼합, 가열, 캐스팅과 같은 단순한 공정들이 상온 조건에서 진행되기 때문에 이 공정은 간편하며 무독성의 특성을 지니며 가격 경쟁력을 갖고 있다. (2) 겔의 크기와 두께를 포함한 모양은 면도날과 유리 블록을 이용해 용이하게 조절 가능하다. 더불어 앞서 언급한 도구들을 이용해 합성된 겔을 유리, 스테인리스 스틸, 플라스틱 판과 같은 서브스트레이트 상에 자유롭게 부착 가능하여 산업적인 확장 가능성을 내포하고 있다. (3) 본 연구에서 합성한 겔과 고분자 집전 장치의 조합을 통해 플렉서블한 슈퍼커패시터를 구현할 수 있다. 이런 장점들로 미루어보아, 겔 합성을 기반으로 한 슈퍼커패시터 제조는 추후 플렉서블 장비 개발에 있어 적합한 원천 기술이 될 것으로

예상된다.

앞서 언급한 공정에 기반하여 한천-염화나트륨 겔 전해질을 적용한 슈퍼커패시터를 제조하였다. 합성된 한천 겔은 3차원적으로 상호연결된 아가로스 구조체와 그 간극에 존재하는 수분과 염화나트륨을 함유한 준-마이크로 크기의 다공성 구조로 이루어져 있다. 지지체로서 아가로스 구조체는 겔 전해질의 구조적 안정성을 유지한다. 더불어, 수분이 포함된 다공성 네트워크는 음극과 양극 사이의 효율적인 이온 수송 통로의 역할을 수행한다. 이런 특징들로 말미암아, 이산화망간 전극과 준-고상 전해질로 구성된 슈퍼커패시터는 286.9 F g^{-1} 의 용량과 같은 농도의 염화나트륨을 함유한 액상 전해질과 비교해 보았을 때 주사 속도 100 mV s^{-1}에서 약 80 퍼센트의 출력 특성을 나타내었다. 이런 좋은 커패시터 성능 특성과 더불어 겔 전해질은 간편한 생산 공정과 한천과 염화나트륨의 구성으로 말미암아 양산을 통해 가격경쟁력 확보가 가능하며 친환경적이며 안전하다. 따라서, 본 연구에서 개발한 준-고상 겔은 추후 에너지 저장 장비의 개발에 있어 중추적인 역할을 할 수 있는 물질로 자리매김 할 것으로 예상된다.

주요어: 전기화학, 슈퍼캐퍼시터, 준고상 겔 전해질, 한천 하이드로겔
학 번: 2013-22522